Biometry of phakic intraocular lens using Scheimpflug photography

Joris E. Coppens, MSc, Thomas J.T.P. van den Berg, PhD, Camille J. Budo, MD

PURPOSE: To examine lateral and axial positioning of phakic intraocular lenses (IOLs) with iris fixation in the anterior chamber and to examine short-term stability of the IOL position.

SETTING: The Netherlands Opthalmic Research Institute, Amsterdam, the Netherlands.

METHODS: Thirty patients participated in the study. Thirty-one eyes were implanted with the 204 type myopia IOL, 14 eyes with the 206 myopia IOL, and 8 eyes with the 203 hyperopia IOL. Scheimpflug slitlamp photographs were made through the optical axis along 4 meridians of the eyes. Ray tracing was used to obtain the lateral and axial position of the IOLs.

RESULTS: Centration of the IOL with respect to the pupil's center and the tilt angle of the IOL with respect to the optical axis of the eye were measured. Standard deviation of decentration was 0.21 mm vertically and 0.16 mm horizontally. Standard deviation of tilt was 1.30 degrees vertically and 0.90 degrees horizontally. Tilt and decentration are proportional to each other. Vaulting, the distance between the crystalline lens and the IOL, was constant over a period of 24 months, ranging from 0.2 to 0.8 mm, depending primarily on the radius of curvature of the crystalline lens. A geometric model for this dependence was formulated.

CONCLUSION: Phakic IOLs with iris fixation can be positioned in the eye with submillimeter precision. Axial position of iris-fixated phakic IOLs over time is excellent. Axial position and vaulting can be predicted when the radius of curvature of the crystalline lens is known. The IOL behaves as if mounted slightly above a sphere—the anterior surface of the crystalline lens.

J Cataract Refract Surg 2005; 31:1904–1914 © 2005 ASCRS and ESCRS

Phakic intraocular lenses (IOLs) have proved to be a good alternative for surgical correction of myopic, hyperopic, and astigmatic refractive errors of the eye.[1–3] One approach is implantation of the Artisan phakic IOL (Ophtec BV). This phakic IOL is placed in the anterior chamber and fixated to the midperipheral iris stroma by pincer-like claws. The first such device, originally called the iris-claw lens, was introduced in 1978 by Worst for the correction of aphakia during cataract surgery. Later, models were developed for the correction of myopia and hyperopia in phakic eyes.

The optical function of an IOL depends on its exact location in the eye. For instance, the distance from the corneal apex to the IOL determines the power needed for optimal correction. Also, decentration and tilt are important for the optical functioning of the IOL. A decentered IOL will increase the risk for halos in scotopic conditions, and tilt may introduce aberrations.

The Artisan phakic IOL is fixated to the surface of the iris, a biological structure of variable shape. There are questions about this method of fixation, especially in terms of the detailed geometric positioning of the IOL. Thus, an inventory of this positioning was made and the results analyzed for the rules of variation.

An optical technique was used to determine IOL positioning. A slitlamp biomicroscope with improved depth of

Accepted for publication March 12, 2005.

From the Netherlands Ophthalmic Research Institute of the Royal Academy of Arts and Sciences (Coppens, van den Berg), Amsterdam, the Netherlands, and Budo-Oogheelkunde (Budo), Sint-Truiden, Belgium.

Supported in part by the Dutch Foundation for Technical Sciences STW (Coppens).

Dr. Budo is a consultant to Ophtec B.V. No other author has a financial or proprietary interest in any material or methods mentioned.

B. Everts (Ophtec) provided detailed information on the geometry of Artisan IOLs.

Reprint requests Joris E. Coppens, MSc, The Netherlands Ophthalmic Research Institute, Meibergdreef 47, 1105 BA Amsterdam, The Netherlands. E-mail: j.coppens@ioi.knaw.nl.

0886-3350/05/$-see front matter
doi:10.1016/j.jcrs.2005.03.078

field was used, following the Scheimpflug principle. With this principle, a cross-sectional image of the anterior eye segment that is entirely in focus can be made. Using this noninvasive technique, high-resolution cross-sectional images were made of eyes with an Artisan phakic IOL. Part of the study objective was to develop a technique for accurate assessment of the position of IOLs with the Scheimpflug camera.

PATIENTS AND METHODS

Patient Population

Thirty consecutive patients participated in the study. Thirty-one eyes were implanted with the Artisan type 204 myopia IOL, 14 eyes with the 206 myopia IOL, and 8 eyes with the 203 hyperopia IOL. The 204 type IOL has 6.0 mm diameter optics; all other models have 5.0 mm diameter optics. Details of these lenses, inclusion and exclusion criteria for this kind of surgery, and the surgical procedure have been presented.[2] One author (C.J.B.) treated all patients in the study. All patients had preoperative and postoperative examinations according to the standard protocol for this surgical procedure.[2] To investigate positional stability of the iris fixation, further examinations were scheduled 6, 12, and 24 months postoperatively. At these postoperative examinations, 24, 14, and 11 patients were measured, respectively.

Intraocular Lens Geometry

Posterior geometry of Artisan IOLs is virtually constant per type. Parameters of the posterior geometry of the IOLs are summarized in Table 1. Changes in spherical power of these IOLs are obtained by varying the radius of curvature of the anterior surface of the IOL. The anterior surface is made in steps of 1.0 diopter (D); minor steps of 0.5 D are obtained by a slightly different radius of curvature of the posterior surface. Figure 1 shows the geometry of the 3 types of IOL involved in this study (top and middle rows) and a schematic for the location of these IOLs when implanted in an eye with a radius of curvature of the anterior surface of the crystalline lens of 10.0 mm (bottom row).

Table 1. Summary of geometry of Artisan lenses.

	IOL Type		
IOL Geometry	203	204	206
Optic diameter (mm)			
Anterior	5.00	6.00	5.00
Posterior	6.20	7.00	6.20
Base vaulting (V_0) (mm)	0.60	0.73	0.82
Claw distance (H_c) (mm)	8.50	8.50	8.50
Haptic area (mm^2)	3.30	1.25	3.30
Mean haptic distance (D_h) (mm)	7.35	7.75	7.35
Posterior radius (R_p (mm) × .0 D/× .5 D)	−8.21/ −8.43	−8.67/ −8.43	−6.24/ −6.12

Measurement Device

Images were recorded with the Nidek EAS-1000 anterior eye segment analysis device.[4,5] This device can produce slitlamp images that are completely in focus by applying Scheimpflug's principle.[6,7] A monochrome charge-coupled device (CCD) camera yields images 640 × 400 pixels wide with an 8-bit dynamic range. The width of the slit source is fixed at 0.08 mm. The length of the slit source is adjustable and was set at 10.0 mm. This length was a compromise to prevent problems with overexposure of the picture due to backscatter of the iris, yet yield as much data as possible for an accurate determination of corneal shape. The combination slitprojector and camera can rotate along the horizontal axis, from 0 to 180 degrees in a clockwise rotation, allowing measurements to be taken at various meridians. Cross-sectional images were recorded at a vertical (0 degree) and horizontal (90 degrees) meridian. Furthermore, 2 diagonal meridians (45 degrees and 135 degrees) were used to create a redundant data set. Alignment of the Scheimpflug camera is done with infrared light; the actual image is recorded during exposure with a xenon flashtube. This tube, in combination with the CCD camera, has a relatively flat spectral response from 450 to 650 nm. Images were made in a dark room; no mydriatic agent was used because natural pupil diameter appeared to be sufficiently large to extract the biometrical data needed for this study. Fixation of the eyes on the optical axis was obtained using an internal fixation target of the device. This target has a vergence of 1 m, requiring the subjects to fixate and accommodate at approximately 1 m distance.

Image Analysis

Normal slitlamp images are strongly distorted because of the perspective view created by the angle between object and image plane and because of the refracting properties of the eye. In 1904, Scheimpflug patented a photographic method to correct for most of the distortion and focus errors seen when a flat object, such as the facade of a building, is viewed from an angle. Scheimpflug images are not only distorted by the geometry of the imaging device but also by the refracting properties of the eye.[8–10] The design of the Nidek EAS-1000 was optimized for minimal distortion due to the imaging geometry of the biomicroscope by using a so-called anamorphous lens system. The main distortion in the Scheimpflug images is due to the optics of the eye. This distortion is large and must be corrected with image-processing techniques.

The first step in the analysis involved detection of the edges of the refracting elements: anterior and posterior corneal surfaces, anterior and posterior surfaces of the IOL, and anterior surface of the crystalline lens. The edge pixels were then used to fit a circle to the surface using an approximate mean square algorithm.[11] This algorithm has been shown to be least sensitive to bias caused by the limited subtended angle of the arc given by the edge pixels. To correct for distortion due to refraction at the ocular surfaces a ray-tracing technique was used. In short, this technique follows the following steps: each pixel in the image is assigned to a ray defined initially by the location of the pixel in the cross-sectional image and the nodal point of the Scheimpflug optics. The ocular surfaces were approximated by spheres that are defined as figures of revolution of the fitted circles. Then, starting from the nodal point, for each ray, the intersection with the anterior corneal surface is determined. At the intersection with the anterior corneal surface, it was redirected according to Snell's law. Refractive index of the cornea was set at 1.376, of the aqueous at 1.336, and of the

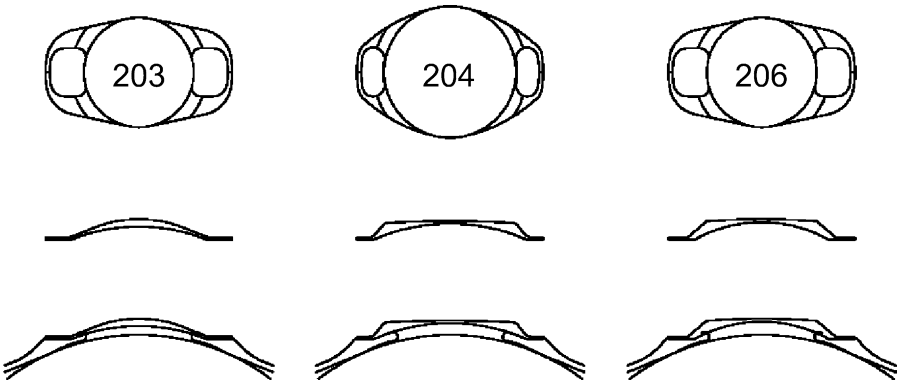

Figure 1. Geometry of Artisan phakic IOLs. *Top*: Top-down view of Artisan phakic IOLs. *Middle*: Cross-section of the IOLs. *Bottom*: Artist's rendering of the position of IOLs on the IOL–iris complex of a typical eye. Anterior surface of the crystalline lens was given a radius of curvature of 10.0 mm.

IOL at 1.49. Subsequently, the rays were traced to parts deeper in the eye in a similar way until they intersected the object (slit) plane. For each pixel in the image, its position in the object plane is now known. Figure 2 gives an example of an image before (*left*) and after (*right*) corrections have been applied. The most important distortion is caused by the anterior surface of the cornea. This surface acts as a kind of magnifying glass for the inner structures of the eye. The crystalline lens, for example, is too large in a raw image. The thickness of the cornea, on the other hand, is too small in a raw image because of the jump in index of refraction from outside (n = 1.000) to cornea (n = 1.376).

The detection of the edges of the refractive elements was done using automatic edge detection algorithms. However, this was not always possible because of insufficient contrast, and all images were inspected by eye. In particular, the surfaces of the IOLs were, as a rule, very faint in the pictures. Evidently, the amount of backscatter from the surfaces of the IOLs is small compared with the backscatter from the biological structures. Therefore, these surfaces were identified manually with 3 points on the edge in an enlarged image. Corneal surfaces were identified manually when automatic edge detection failed on occasion. In the final analysis, all good-quality images were used.

Axes

The Nidek EAS-1000 contains 2 internal fixation lights, 1 on the optical axis of the device and 1 with a 4-degree nasal and 1-degree upward offset. The latter was used in this investigation. It gives cross-sections along the optical axis of the eye rather than along the visual axis. Proper lateral position of the eye is achieved by alignment of the first Purkinje image on the optical axis of the instrument. For this study, the optical axis of the crystalline lens was chosen as reference. In the recorded images, the optical axis of the crystalline lens can be defined as the line of symmetry through the eye lens. This was found as the line through the center

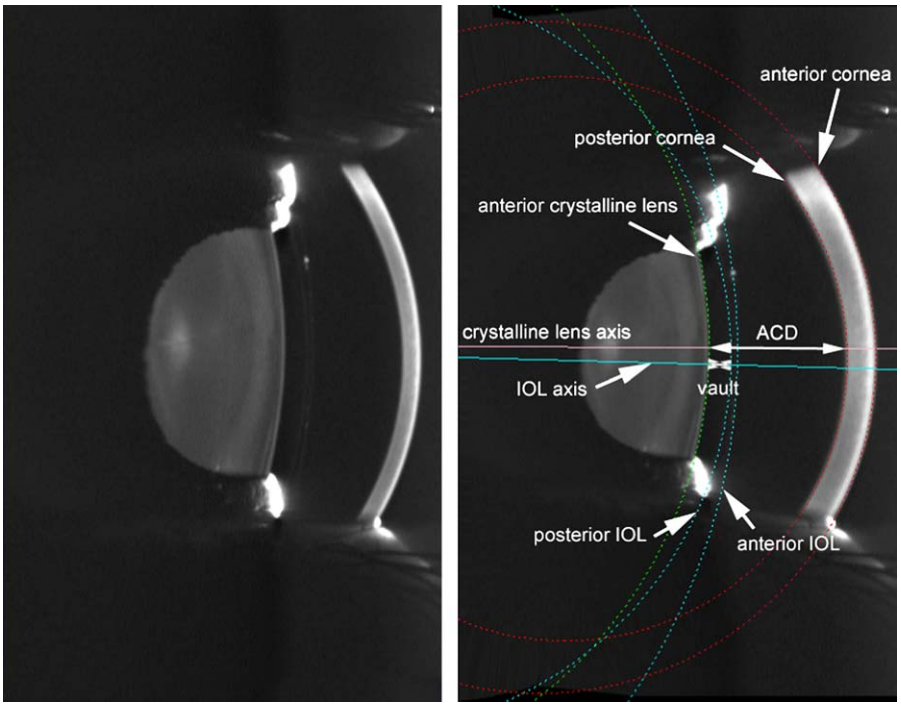

Figure 2. *Left*: Typical example of a vertical cross-section made with the EAS-1000 Scheimpflug camera. The anterior and posterior surfaces of the IOL are faintly visible. *Right*: The same image after processing. Edges of the refracting elements are indicated with dashed circles; optical axes of the eye and the IOL are indicated with continuous lines.

of the circle fitted to the anterior surface of the crystalline lens, bisecting the symmetry in the inner structure of the crystalline lens. This symmetry was indicated by hand, judging the symmetry structure of the crystalline lens by eye. For this symmetry detection, an automatic procedure was attempted first, but this proved unreliable.

In the recorded images, the optical axis of the IOL can be found as the line through the centers of the circles fitted to the anterior and the posterior surfaces of the IOL. Tilt (orientation) of the IOL is calculated as the angle between the optical axis of the crystalline lens and the axis of the IOL. Decentration is defined as the distance between both axes at the level of the anterior surface of the crystalline lens.

Combination of Meridians

In each of the 4 Scheimpflug camera orientations (0, 45, 90, and 135 degrees), pictures were taken and values for tilt and decentration were derived as explained earlier. This was a redundant set because, for example, only tilt and decentration in the 0-degree and 90-degree meridians would be sufficient. In this study, this redundancy was used to test consistency. In the final analysis, all available data were used. Values for tilt and decentration are all presented by their vertical (0-degree) and horizontal (90-degree) components. To express the 45-degree and 135-degree diagonal measurements in their vertical (0-degree) and horizontal (90-degree) components, the following equations were used:

$$q_0 = \frac{q_{45} - q_{135}}{\sqrt{2}}, q_{90} = \frac{q_{45} + q_{135}}{\sqrt{2}},$$

with q_φ the quantity measured at meridian φ.

Model for Vaulting

The distance between the posterior surface of the phakic IOL and the anterior surface of the crystalline lens (on its optical axis) is referred to as "vaulting." Part of the objective of this study was to understand the origins of differences in vaulting distances among people and IOL types. A simple geometric model is proposed as a first attempt to better understand the mechanisms involved in the vaulting distance of iris-fixated phakic IOLs. This model is illustrated in Figure 3.

The upper and middle parts of Figure 3 show geometrical properties of the IOL, of importance for this model. The measurements D_c,V_0, and R_p were directly obtained from the data sheets of the lenses. D_h was introduced as a new measure. This value is the average effective distance of the haptics. Note that fixation is by means of a piece of iris tissue, held in the claws, pulling the footplate of the haptics against the iris. The footplate presses against the iris as counterforce for the enclavated piece of iris. D_h is the distance between the 2 points where this counterforce effectively acts. In this study, it is assumed that D_h is equal to the geometric mean of the haptic distance.

The lower part of Figure 3 shows a schematic cross-section of the anterior segment of an eye with an Artisan IOL (type 206 high myopia, 5 mm diameter optics). The vaulting distance is indicated as V, and the radius of curvature of the anterior surface of the crystalline lens is indicated as R_a. The figure suggests that the vaulting distance decreases with a smaller radius of curvature of the anterior surface of the crystalline lens, if it is assumed that the shape of the iris depends on the curvature of the anterior surface of the lens. Using the geometry in Figure 3, the following equation can be found:

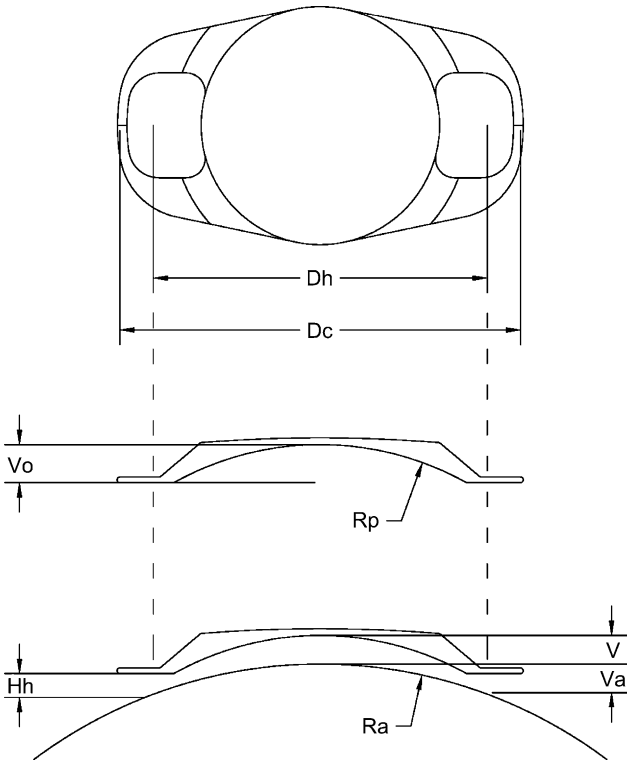

Figure 3. *Top*: Top-down view of an Artisan phakic IOL. D_c is the claw distance and D_h, the average distance of the haptics, the flat footplate of the phakic IOL. *Middle*: Cross-section of a phakic IOL. Base vaulting of the posterior surface is indicated as V_0; radius of curvature of the posterior IOL surface is R_p. *Bottom*: Position of the IOL with respect to the anterior surface of the crystalline lens. V is the vaulting distance; V_a is the vertical distance between 2 points of the anterior surface of the crystalline lens: (1) at the center and (2) at the effective (average) location of the haptics. H_h is the distance between the posterior surface of the haptics and the crystalline lens, at the position D_h.

$$V = V_0 + H_h - V_a = V_0 + H_h - R_a\left[1 - \cos\left(\arcsin\left(\frac{D_h}{2R_a}\right)\right)\right], \quad (1)$$

which can be simplified in first-order approximation to

$$V = V_0 + H_h - \frac{D_h^2}{8}\frac{1}{R_a}, \text{under the assumption } D_h << R_a. \quad (2)$$

Initial data analysis was done using Equation 2. However, because the assumption $D_h << R_a$ is not rigidly valid, all results reported were obtained using Equation 1.

RESULTS

Lateral Position

During the recording sessions, the operator carefully checked for quality of the recordings and repeated the measurement if the image proved to be faulty because of bad fixation, lid closure, or other factors. With the camera used for this study, it was not possible to achieve proper recordings at all orientations for all patients. Especially at 90 degrees, eyelashes often obstructed the measurements; it was easiest to obtain a good recording at 0 degree. Changes over time, if any, were too insignificant to consider in this analysis. For the following results, all available postoperative recordings were used.

Decentration

Figure 4 shows the comparison between the 0/90-degree and the 45/135-degree data sets. Along the *x* axis, the decentration is shown as it followed directly from the 0-degree and 90-degree recordings. On the *y* axis, the decentration is shown as found by calculation from the 45-degree and 135-degree recordings. The points shown are the average per eye of all postoperative measurements available. The error bars indicate the standard error of the mean. Data points without error bars are shown if only a single measurement was available. The points seem to be randomly distributed around the line $y = x$ shown in the plot. This indicates that the data set obtained from the vertical and horizontal recordings can be considered more or less equivalent to the set obtained from the diagonal recordings. To reduce the random error in the measurement outcomes, both data sets were averaged in the further analysis.

Figure 5 shows the decentration in the right eyes and the left eyes. Both plots show a tendency for the IOLs to be positioned slightly downward and nasally. In the right eyes, the mean vertical position was -0.09 ± 0.03 mm and the horizontal, $+0.03 \pm 0.03$ mm (mean $\pm$ SE). In the left eyes, the mean vertical position was -0.16 ± 0.04 mm and the horizontal, -0.12 ± 0.03 mm.

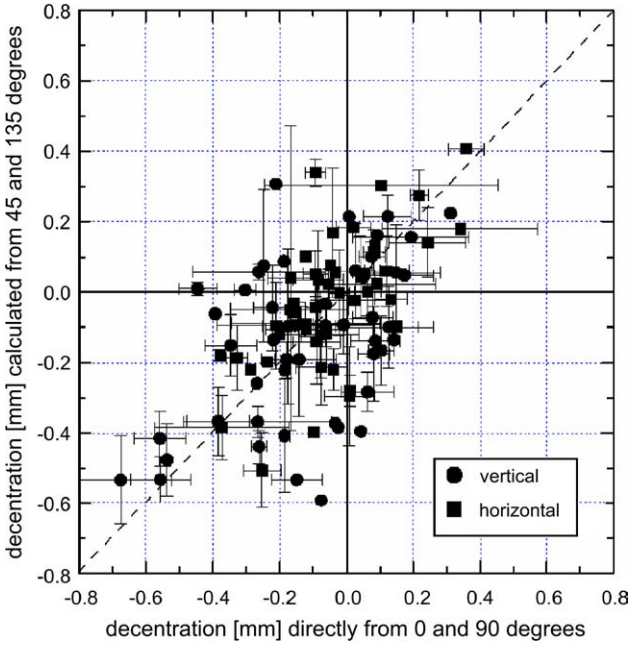

Figure 4. Intraocular lens decentration as directly measured vertically (0 degree) and horizontally (90 degrees) is plotted on the *x*-axis, and the same data but now reconstructed from the oblique (45-degree and 135-degree) measurements on the *y*-axis. Vertical decentration is indicated with circles and horizontal decentration with squares.

Tilt

Figures 6 and 7 are plots similar to Figures 4 and 5 but are related to IOL tilt. Figure 6 gives the comparison of the 0/90-degree and the 45/135-degree data sets. On the *y* axis,

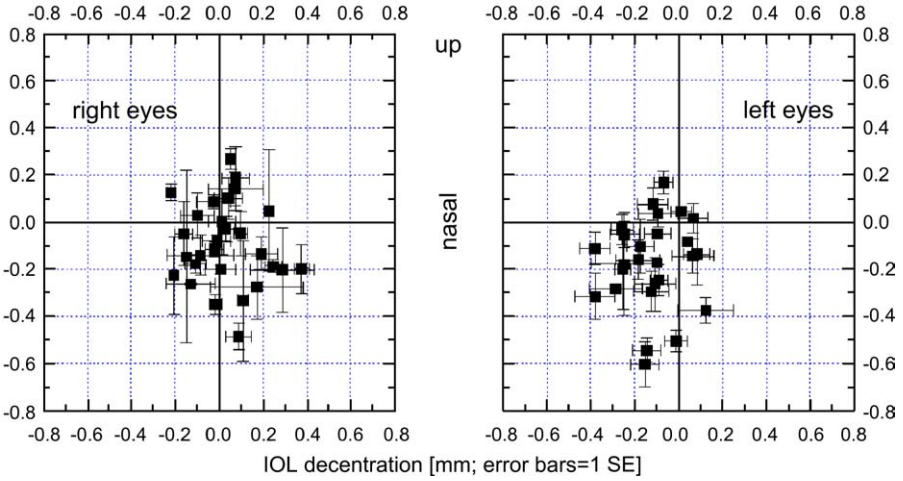

Figure 5. Decentration of the IOLs in a vector diagram, showing horizontal decentration on the *x* axis and vertical decentration on the *y* axis. Data from all meridians and all available postoperative measurements are used. Error bars indicate standard errors.

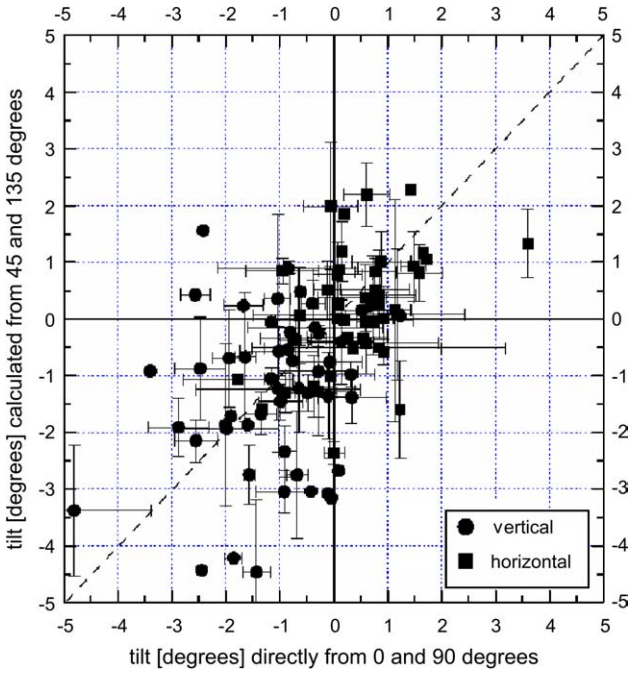

Figure 6. Comparable to Figure 4 but now showing IOL orientation (tilt) instead of decentration. On the *x* axis, the tilt from the vertical (0-degree) and horizontal (90-degree) measurements is shown; on the *y* axis, the same is shown but now calculated from linear combinations of the diagonal (45-degree and 135-degree) measurements.

the tilt data obtained from combinations of the diagonal data into the vertical and horizontal components is shown; on the *x* axis, the tilt data were obtained directly from the vertical and horizontal recordings. Again, the data scatter around the line $y = x$, so the 0/90-degree and the 45/135-degree data sets can be considered more or less equivalent. Error bars indicate the standard errors obtained from measurements of all available postoperative measurements. For tilt, the data from the 0/90-degree and the 45/135-degree data sets were combined in the further analysis.

Figure 7 shows the tilt of the IOLs in the right and left eyes. The tilts tended to be downward and nasally, as was the case for decentration. In the right eyes, the mean vertical tilt was -1.2 ± 0.2 degrees and the mean horizontal tilt, -0.1 ± 0.2 degrees (mean $\pm$ SE). In the left eyes, the mean vertical tilt was -1.3 ± 0.3 degrees and the mean horizontal tilt, -0.6 ± 0.2.

Relation Between Decentration and Tilt

In Figure 8, the decentration in the vertical and horizontal meridians is shown as a function of the tilt. The data points are shown for both eyes. Each data point is based on all available Scheimpflug images for that eye. Error bars indicate the standard error of the mean. Data points without error bars are from a single measurement. Both the vertical and the horizontal data clearly show that a positive correlation exists between tilt and decentration. An IOL that is decentered downward tends to "point" downward; one that is decentered nasally tends to "point" nasally. Figure 8 suggests that proportionality exists between decentration and tilt, with a proportionality factor of about 0.15 mm/degree. This proportionality points toward the following model: If it is assumed that the relation between centration and orientation can be modeled as if the IOL is placed on a sphere, then for small decentrations, the following relation holds: $r = \frac{180d}{\pi\theta}$, where r is the radius of the sphere (in mm), d the decentration (in mm) and θ the tilt (in degrees). The ratio of decentration and tilt is calculated as major axis regression, given by the ratio of the standard deviation of decentration and standard deviation of tilt. Numerical results are summarized in Table 2.

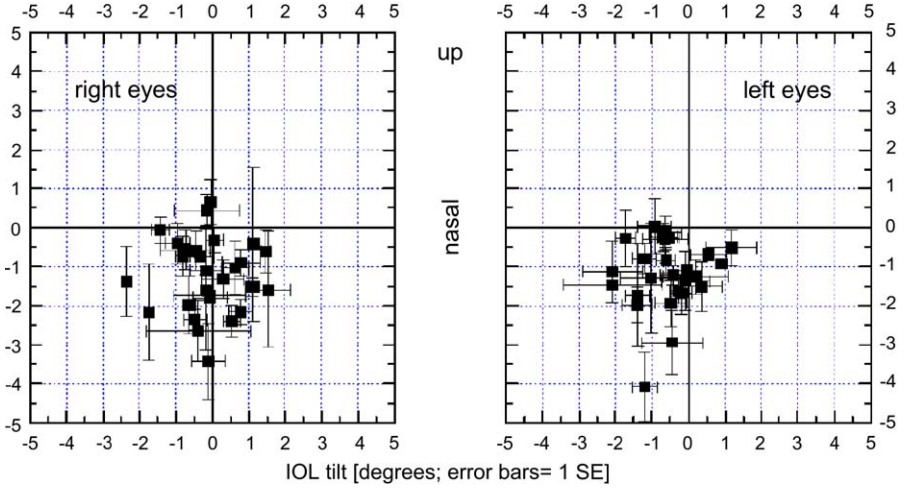

Figure 7. Comparable to Figure 5 but now showing tilt. Vector diagram showing the horizontal tilt on the *x*-axis and the vertical tilt on the *y*-axis. Error bars are standard errors.

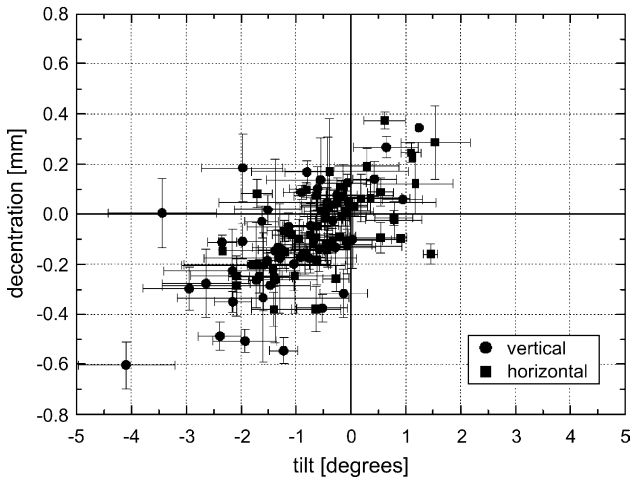

Figure 8. Relation between decentration and tilt. Decentration is plotted on the *y*-axis versus tilt on the *x*-axis both for the vertical (square) and horizontal (circle) meridian.

Axial Position and Positional Stability

Anterior chamber depth, defined as the geometrical distance, in millimeters, between apex of the posterior cornea and apex of the anterior crystalline lens, was derived from the data, as explained above. Results are given in Figure 9, in which postoperative data are plotted against the preoperative data. No systematic change in anterior chamber depth was found between preoperative and postoperative data. Later postoperative follow-up data also showed no change in anterior chamber depth. This result may serve as a check to ensure that proper image processing procedures were used. Furthermore, it shows that the IOL did not affect the position of the crystalline lens.

Table 2. Summary of lateral positioning.

	Meridian	
	Vertical (0°)	Horizontal (90°)
Mean decentration (mm)	−0.12	0.07 nasally
Population SD decentration (mm)	0.21	0.16
Repeated-measures SD decentration (mm)	0.09	0.07
Mean tilt (degree)	−1.24	0.33 nasally
Population SD tilt (degree)	1.3	0.90
Repeated-measures SD tilt (degree)	0.6	0.5
Radius (corr. decentration tilt) (mm)	9.1	10.3
Pearson *r* (decentration tilt)	0.64	0.59
Number of observations	58	54
P (2 tailed)	<.001	<.001

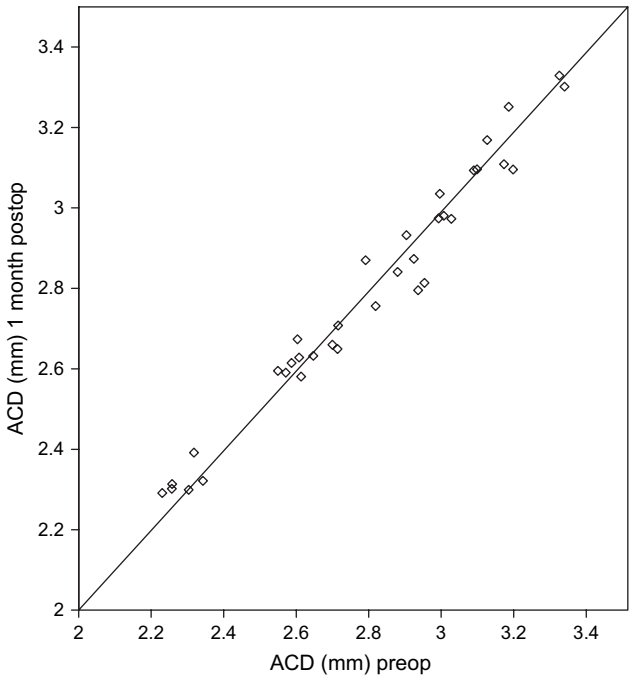

Figure 9. Anterior chamber depth measured 1 month postoperatively versus preoperatively obtained from 0-degree images. No systematic change was found.

Vaulting Distance

Vaulting distances are shown in Figure 10. Vaulting data in the first 4 postoperative measurements is shown, with data of session n+1 (po 2, po 3, po 4) plotted against those of session n (po 1, po 2, po 3). The data show no systematic change in vaulting distances between sessions. A summary of the numerical data of ACD and vaulting is given in Table 3.

To understand why such a wide variation of vaulting distances was found in our data set, various parameters were analyzed. The dominant parameter appeared to be the radius of curvature of the anterior surface of the crystalline lens. This led to the model for vaulting, described above. According to the model, vaulting distance in first-order approximation is linearly related to the reciprocal of the radius of curvature of the anterior surface of the crystalline lens.

The vaulting distance was fitted to the radius of curvature of the anterior surface of the crystalline lens, using Equation 1. With V_0 (the vault for a lens on a flat surface) fixed, according to Table 1, the parameters H_h (vertical distance between haptic and crystalline lens) and D_h (effective haptic diameter) resulted. Because the various types of Artisan IOLs might behave differently, partially because of different geometry of the posterior surface, data were sorted according to IOL type and fitted independently. Data

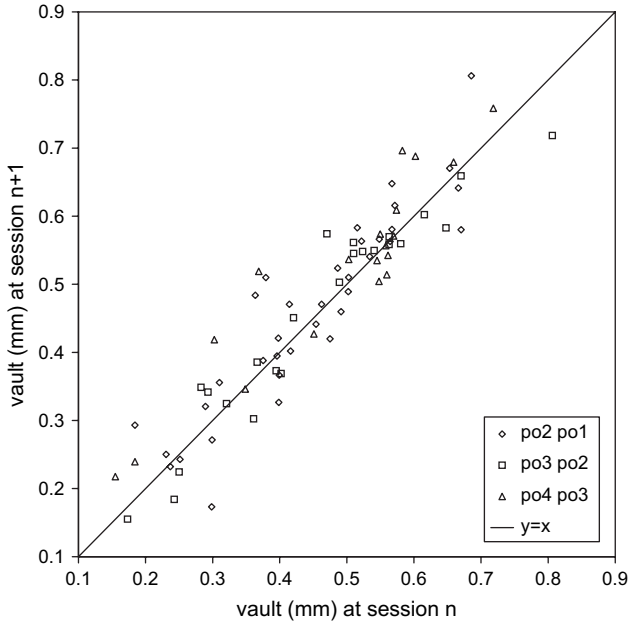

Figure 10. Vaulting distances as obtained from vertical (0-degree meridian) images for the first 4 postoperative measurement sessions.

from all available postoperative images, at all 4 angles, were averaged per eye.

Figure 11 shows the data for the type 203 (5.0 mm diameter optics) hyperopic IOL, the type 204 (6.0 mm diameter optics) myopic IOL, and the type 206 (5.0 mm diameter optics) high myopic IOL. Error bars indicate standard errors. Also shown in the figure are the lines fitted to the model in Equation 1. Results of the fit are summarized in Table 4.

It can be seen that the fitted values of D_h were not far from the values calculated on the basis of the geometry as explained in Patients and Methods. To further test the vaulting model, D_h was derived from known geometric parameters of the IOLs, and fixed at the values shown in Table 1 and repeated in Table 5. H_h values were then optimized again for least sum of squared differences between measured and modeled data. Results are shown in Figure 12. The residuals of this fit showed no significant correlation with measured data, indicating that assumed values for D_h are valid.

DISCUSSION

The Scheimpflug images appeared to be well suited to reconstruction of anterior chamber geometry. Although this technique was not intended for the measurement of phakic IOLs because these lenses have no internal scattering structure, the backscatter from the IOL surfaces appeared to be sufficient for detection. Measurement error (repeated-measures SD) was shown to be on the order of 0.2 mm for decentration and 1 degree for tilt, which provides good accuracy. However, the systematic effects that were found in decentration and tilt proved to be small—in fact, of the same order as this measurement error. For this reason, we had to combine as many data as possible to reach statistical significance for the systematic effects.

Availability of data was determined first by the number of recording sessions for an eye. Second, not all recordings were of equal quality. Some at the horizontal and diagonal meridians could not be used because of vignetting from eyelashes and eyebrows. Long eyelashes may interrupt the detected edges of the anterior of the crystalline lens or, in worse cases, even the edges of the cornea. In these cases, the corneal edge had to be indicated manually, resulting in reduced accuracy. Some of the patients had such pronounced eyebrows that only part of the cornea could be recorded in the horizontal meridian; deeper structures of the eye could not be visualized with the EAS-1000 under these circumstances. Apart from the availability and quality of data, the accuracy of centration measurement with the Scheimpflug technique depends on the power of the IOL. The higher the power of the IOL, the higher the difference in radius of curvature between posterior and anterior surfaces of the IOL; therefore, the center was better defined for high-power IOLs. Accuracy of the combined measurements is sufficient to conclude that the IOLs are positioned in the eye with precision of a tenth of a millimeter.

Table 3. Stability of axial position.

	Sessions			
Measurements	PO1–Preop	PO2–PO1	PO3–PO2	PO4–PO3
Mean anterior chamber depth (mm)	−0.005	−0.008	−0.008	−0.015
SE anterior chamber depth (mm)	0.008	0.010	0.008	0.010
Mean vault		−0.013	−0.000	0.012
SE vault		0.021	0.009	0.022
Number of observations	42	38	24	20

PO = postoperative; Preop = preoperative; SE = spherical equivalent

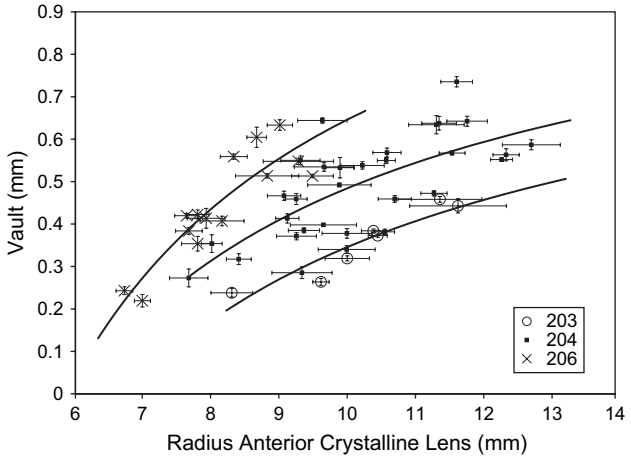

Figure 11. Vaulting distances for 3 types of iris-fixated phakic IOLs as function of the radius of the curvature of the anterior surface of the crystalline lens. All available postoperative data per eye were averaged. Error bars are ± SE. Lines show the result of a fit to Equation 2, with D_h and H_h as free parameters per type of IOL.

We wondered about the laws that govern the position of the phakic IOL. Although the positioning errors were small, these errors could be used as an "experiment of nature." The most striking result is shown in Figure 8. Tilt and decentration seem to be closely proportional in this figure, especially taking into account the measurement variability, as indicated with the error bars. This can be modeled as if the IOL is implanted on a sphere with a radius of curvature of about 10.0 mm. This might correspond to the mean shape of the iris because it is curved over the anterior surface of the crystalline lens. The anterior surface of the crystalline lens in this population has a mean radius of 10.0 mm.

Within this model of proportionality between tilt and decentration, there is a tendency for the IOLs to be decentered and tilted downward and perhaps slightly nasally. One might speculate whether gravity causes this effect. The specific weight of the IOL (1.19 kg/L), and also that

Table 4. Results of model fit with D_h free.

	IOL Type		
Parameter	203	204	206
H_h (fit result) (mm)	0.38	0.38	0.58
D_h (fit result) (mm)	7.0	7.0	7.6
V_0 (fixed) (mm)	0.60	0.73	0.82
R^2 (fit result)	0.86	0.50	0.80
Residual SD (mm)	0.032	0.084	0.055

D_h = mean haptic distance; H_h = distance between posterior surface of the haptics and the crystalline lens; IOL = intraocular lens; V_0 = base vaulting

Table 5. Results of fit with D_h fixed.

	IOL Type		
Parameter	203	204	206
H_h (fit result) (mm)	0.44	0.54	0.51
D_h (fixed) (mm)	7.35	7.75	7.35
V_0 (fixed) (mm)	0.60	0.73	0.82
R^2 (fit result)	0.86	0.50	0.80
Residual SD (mm)	0.033	0.087	0.056

D_h = mean haptic distance; H_h = distance between posterior surface of the haptics and the crystalline lens; IOL = intraocular lens; V_0 = base vaulting

of the iris, is higher than that of the aqueous humor, and the surgery is performed with the patient in the supine position, whereas photography is performed with the patient in the upright position. Moreover, scrutiny of Figure 8 also shows that this tilt is, on average, a little bit more than follows from the proportionality with decentration, according to the sphere model. The cloud of data points in Figure 8 is slightly shifted to the left with respect to this proportionality law. The pincer-like claws of the IOLs could act as a kind of hinge, allowing some freedom in vertical orientation and causing a little extra tilt. This finding is confirmed in the literature[12]; after pupil dilation, biomicroscopy seemed to indicate a tilt of the Artisan IOL, which appeared to pivot around the horizontal axis under the influence of gravity.

Apart from these systematic effects, other sources of variability could play a role. Comparison of tilt and

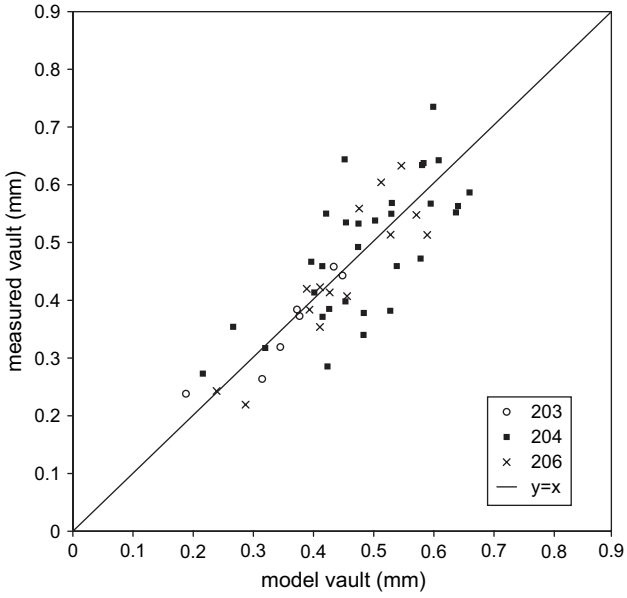

Figure 12. Measured vault plotted against vault calculated with the geometrical model and the H_h values obtained from the fit (Table 3).

decentration of the left and right eyes showed no significant correlations. This indicated that the variation is independent of the patient. Some of the variation may be related to pupil size. It is known that the center of the pupil shifts, more or less randomly, by a few tenths of a millimeter for different states of dilation.[13,14] During implantation of phakic IOLs, miotic drops are applied to prepare the iris for lens fixation and to reduce the risk of lens touch during the surgery.[2] During photography, however, which was done in relative darkness, the mean pupil size was about 6.0 mm. Apart from these sources of variation by nature, variation because of the surgery must also be considered. However, it was not possible to assess this source of variation separately in this study.

Because the iris is such delicate and motile tissue, its suitability to fixate an IOL must be considered. This study has shown that there is no indication of positional change of iris-fixated phakic IOLs over a period of 24 months. Thus, iris fixation appears to be stable, which is in agreement with another study that included iris-fixated phakic IOLs.[15]

Apart from stability, the question of which laws govern axial position of an iris-fixated phakic IOL remains. Axial position of an IOL in the anterior chamber of an eye is important. First, sufficient space between an IOL and the crystalline lens to allow free flow of aqueous humor is necessary. Additionally, the distance between the IOL and the corneal endothelium must be sufficiently large to prevent risk of endothelial cell loss. Apart from these, the axial position of an IOL must be known for calculations of the refractive effect.

A geometric model was proposed to predict the axial position of a phakic IOL based on the geometry of the IOL and the radius of curvature of the anterior surface of the crystalline lens. The model is based on the hypothesis that iris shape follows the shape of the anterior surface of the crystalline lens. On average, this proved to be the case. Otherwise, the fitted D_h values might have deviated systematically from the true ones.

The model was relatively precise at predicting axial position of the 5.0 mm diameter IOLs, with a mean residual error of 0.045 mm for the 203 and 206 IOL types. Predicted axial position of 6.0 mm diameter IOLs was less accurate, with a residual error of 0.087 mm (Figures 11 and 12). The cause of this difference might be related to the shape of the haptics of the IOL. The 5.0 mm optic types have a much larger haptic footplate (3.3 mm^2) than the 6.0 mm type (1.25 mm^2). A larger footplate gives better defined positioning. To elaborate, suppose the iris fixation behaves as follows: The piece of iris tissue between the claws creates a force toward the rest of the iris tissue. The strength of this elastic force varies between cases. The axial position of the IOL is defined by the pressure of the posterior side of the haptics, providing a counterforce. For a certain counterforce, the pressure on the iris is inversely related to footplate area. Thus, with a smaller haptic area, more variation in axial position is to be expected. In fact, the variation in H_h was on average 0.05 mm for the large haptic models (203 and 206) and 0.09 mm for the small haptic model (204), corresponding to the 3.3 mm^2 versus 1.25 mm^2 footplate area.

According to the model in this article, vaulting distance is dependent on the shape of the crystalline lens. However, in any individual, this shape is not constant. On the contrary, during accommodation, the radius of curvature changes. Data in this study have been recorded at about 1 D accommodation, the vergence of the fixation target; with, for example, 5 D of accommodation, the radius of curvature may change from 12.0 mm to 8.0 mm. This raises the question what happens with the iris-fixated IOL vaulting during accommodation. Vaulting distances might be reduced drastically. Indeed, a case report mentions a severe reduction of vaulting distance at 7 D of accommodation.[12]

It is known that the geometry of the anterior chamber changes with aging. In particular, the radius of the crystalline lens curvature and the anterior chamber depth decrease with age.[10,16] Both these aging effects might reduce the distance between the phakic IOL and tissue of the eye. A decrease in anterior chamber depth might reduce the distance between phakic IOL and corneal endothelium, whereas the decrease of radius of the anterior surface of the crystalline lens might reduce the vaulting distance.

In conclusion, the Artisan phakic IOL can be positioned in the eye with about 0.2 mm precision. The most important rule that applies is a high correlation between decentration and tilt, which is characteristic of iris fixation. In general, there is a slight downward tilt and decentration of the phakic IOL, possibly because of gravitational effects. Iris-claw fixation provides a stable and predictable axial position for the IOL, according to the formulated model. The IOL behaves as if it were mounted slightly above a sphere—the anterior surface of the crystalline lens.

REFERENCES

1. Dick HB, Alió J, Bianchetti M, et al. Toric phakic intraocular lens; European multicenter study. Ophthalmology 2003; 110:150–162
2. Budo C, Hessloehl JC, Izak M, et al. Multicenter study of the Artisan phakic intraocular lens. J Cataract Refract Surg 2000; 26:1163–1171
3. Saxena R, Landesz M, Noordzij B, Luyten GPM. Three-year follow-up of the Artisan phakic intraocular lens for hypermetropia. Ophthalmology 2003; 110:1391–1395
4. Sakamoto Y, Sasaki K. Accuracy of biometrical data obtained from the NIDEK EAS-1000. Ophthalmic Res 1994; 26(suppl):26–32
5. Sakamoto Y, Sasaki K, Nakamura Y, Watanabe N. Reproducibility of data obtained by a newly developed anterior eye segment analysis system, EAS-1000. Ophthalmic Res 1992; 24(suppl):10–20

6. Scheimpflug T. Improved method and apparatus for the systematic alteration or distortion of plane pictures and images by means of lenses and mirrors for photography and for other purposes. British patent no. 1196,1904
7. Drews RC. Depth of field in slit lamp photography; an optical solution using the Scheimpflug principle. Ophthalmologica 1964; 148:143–150
8. Kampfer T, Wegener A, Dragomirescu V, Hockwin O. Improved biometry of the anterior eye segment. Ophthalmic Res 1989; 21: 239–248
9. Huebscher H-J, Fink W, Steinbrück D, Seiler T. Scheimpflug records without distortion—a mythos? Ophthalmic Res 1999; 31:134–139
10. Dubbelman M, van der Heijde GL. The shape of the aging human lens: curvature, equivalent refractive index and the lens paradox. Vis Res 2001; 41:1867–1877
11. Fitzgibbon AW, Fisher RB. A buyer's guide to conic fitting. Proceedings of the British Machine Vision Conference 1995, Birmingham England.
12. Baikoff G, Lutun E, Wei J, Ferraz C. Contact between 3 phakic intraocular lens models and the crystalline lens: an anterior chamber optical coherence tomography study. J Cataract Refract Surg 2004; 30:2007–2012
13. Wilson MA, Campbell MCW, Simonet P. Change of pupil centration with change of illumination and pupil size; the Julius F. Neumueller Award in Optics, 1989. Optom Vis Sci 1992; 69: 129–136
14. Walsh G. The effect of mydriasis on the pupillary centration of the human eye. Ophthalmic Physiol Opt 1988; 8:178–182
15. Baumeister M, Bühren J, Kohnen T. Position of angle-supported, iris-fixated, and ciliary sulcus-implanted myopic phakic intraocular lenses evaluated by Scheimpflug photography. Am J Ophthalmol 2004; 138:723–731
16. Baikoff G, Lutun E, Ferraz C, Wei J. Static and dynamic analysis of the anterior segment with optical coherence tomography. J Cataract Refract Surg 2004; 30:1843–1850